Nanoscale

Synthesis of sub-millimeter single-crystal grains of aligned hexagonal boron nitride on epitaxial Ni film

Journal:	*Nanoscale*
Manuscript ID	NR-ART-04-2019-003525.R1
Article Type:	Paper
Date Submitted by the Author:	17-Jun-2019
Complete List of Authors:	Taslim, Alexandre ; Kyushu University, Interdisciplinary Graduate School of Engineering Sciences Nakajima, Hideaki; National Institute of Advanced Industrial Science and Technology Tsukuba Center Tsukuba Central Lin, Yung-Chang; National Institute of Advanced Industrial Science and Technology Tsukuba Center Tsukuba Central Uchida, Yuki; Kyushu University, Interdisciplinary Graduate School of Engineering Sciences Kawahara, Kenji; Kyushu University, Global Innovation Center (GIC) Okazaki, Toshiya; National Institute of Advanced Industrial Science and Technology Tsukuba Center Tsukuba Central Suenaga, Kazu; National Institute of Advanced Industrial Science and Technology Tsukuba Center Tsukuba Central Hibino, Hiroki; Kwansei Gakuin University Ago, Hiroki; Kyushu University, Global Innovation Center (GIC)

Nanoscale

ARTICLE

Synthesis of sub-millimeter single-crystal grains of aligned hexagonal boron nitride on epitaxial Ni film

Received 00th January 20xx,
Accepted 00th January 20xx

DOI: 10.1039/x0xx00000x

www.rsc.org/

Alexandre Budiman Taslim,[a] Hideaki Nakajima,[b] Yung-Chang Lin,[c] Yuki Uchida,[a] Kenji Kawahara,[d] Toshiya Okazaki,[b] Kazu Suenaga,[c] Hiroki Hibino,[e] and Hiroki Ago*[a,d]

Hexagonal boron nitride (h-BN), an insulating two-dimensional (2D) layered material, has attracted an increased interest due to its electrical screening effect, high-temperature-resistant gas barrier property, and other unique applications. However, the presence of grain boundaries (GBs) in the h-BN hinders to obtain these properties. Here, we demonstrate the epitaxial growth of monolayer h-BN by chemical vapor deposition (CVD) on a Ni(111) thin films deposited on c-plane sapphire. The Ni(111) film showed higher thermal stablity than Cu(111) and Cu-Ni(111) alloy films, allowing to perform the CVD growth at a high temperature of 1100 °C. This resulted in an increase of the h-BN grain sizes to up to 0.5 millimeter, among the highest reported so far, and in a well-defined triangular grain shape. Low-energy electron microscopy (LEEM) revealed the epitaxial relationship between the h-BN and the underlying Ni(111) lattice, leading to a preferential alignment of the h-BN grains. Both the large grain size and the aligment are expected to facilitate the synthesis of h-BN with a low density of GBs. We also found that the addition of N_2 gas during the CVD improves the crystalline shape of the h-BN grains, changing from irregular, truncated to sharp triangle. Growth behavior of monolayer h-BN is further discussed in terms of the dependences on growth temperature and pressure, as well as on the structural evolution of the Ni metal catalyst. Our findings not only help understanding the h-BN growth mechanism but also offer a new route to grow high-quality, monolayer h-BN films.

Introduction

Since the first report on the mechanical exfoliation and successive transport measurement of graphene,[1] atomic sheets of two-dimensional (2D) layered materials have formed a new research field accelerated by the emergence of a wide variety of 2D materials. One of the most important and attractive 2D materials is hexagonal boron nitride (h-BN), called "white graphene", which is insulator with a wide band gap of ~5.9 eV.[2] H-BN has a honeycomb lattice similar to that of graphene, but it has alternating B-N bonds. The polar B-N bonds originated in the different electronegativities of B and N atoms induce the large band gap in h-BN.[3] In addition, h-BN has higher chemical and thermal stability than graphene,[4] while their mechanical properties are comparable.[5]

These unique physical properties of h-BN make it a promising material for applications in various fields, such as deep ultraviolet emitter,[6] magnetic tunnel junction,[7] separator in Li-ion battery,[8] proton separation membrane,[9] and substrate for surface-enhanced Raman spectroscopy.[10] Flexible and transparent hetero-stacked devices composed of h-BN and other 2D materials, such as MoS_2 and WSe_2, have been developed.[11] More importantly, h-BN is regarded as an ideal insulating substrate for graphene and other 2D materials, being able to screen out influences of the underlying substrates, such as surface roughness and optical phonons existing on a SiO_2/Si substrate. This contributes to bring out the intrinsic electrical and optical properties of 2D materials.[12] Theoretical studies suggested that band gap of graphene can be tuned by stacking it on h-BN due to a symmetry breaking effect.[13] The h-BN layers can be also applied as gas barrier film to protect air-sensitive materials, such as black phosphorous (BP).[14] Moreover, h-BN acts as a better anticorrosion barrier than graphene, because graphene partly assists metal corrosion via a cathodic reactions induced by the high electrical conductivity of graphene.[15]

As it is difficult to prepare large and uniform h-BN sheets by mechanical exfoliation,[12] chemical vapor deposition (CVD) methods have been widely used to grow large-area h-BN sheets with relatively low cost.[16] Although h-BN can be directly deposited on insulating substrates, the crystallinity is generally low in the absence of a transition metal catalyst.[17,18] Therefore, various metal catalysts, such as Cu,[19-25] Pt,[26-27] Au,[28] Co,[29] Ir,[30] and Ni,[31] and have been studied to synthesize h-BN.

[a] Interdisciplinary Graduate School of Engineering Sciences, Kyushu University, Fukuoka 816-8580, Japan
[b] CNT Application Research Center, AIST, Tsukuba 305-8565, Japan
[c] Nanomaterials Institute, AIST, Tsukuba 305-8565, Japan
[d] Global Innovation Center (GIC), Kyushu University, Fukuoka 816-8580, Japan
[e] School of Science and Technology, Kwansei Gakuin University, Hyogo 669-1337, Japan

† Footnotes relating to the title and/or authors should appear here.
Electronic Supplementary Information (ESI) available: [details of any supplementary information available should be included here]. See DOI: 10.1039/x0xx00000x

Among them, Cu is the most widely used catalyst, because it gives monolayer h-BN by a mechanism similar to that observed in graphene, where the self-limiting growth can be applied to the selective formation of monolayer graphene.[32] However, the grain size of monolayer h-BN formed on Cu is limited to below 100 μm.[19-25] This gives a number of grain boundaries (GBs) due to merging of small and randomly oriented h-BN grains, deteriorating the mechanical, electrical, and chemical properties of the h-BN.[15,33]

Several studies to increase the grain size of CVD-grown monolayer h-BN have been reported. Pre-oxidation of Cu foil was shown to reduce the nucleation density of h-BN, resulting in the formation of 20 μm-sized h-BN grains.[34] The addition of Ni to Cu, *i.e.* Cu-Ni alloy, was also suggested to reduce the nucleation density by suppressing the formation of poly-aminoborane particles originated in ammonia borane (BH_3NH_3) precursor.[35] These particles act as nucleation sites so that the reduction of the number of these particles can lead to the increased grain size (70-90 μm).[35] A Fe thin film sputtered on Si substrate with a controlled surface SiO_2 layer was shown to give h-BN grains with 300 μm lateral size.[36] However, because polycrystalline metal catalysts are used in these studies, randomly oriented h-BN grains are obtained, giving many GBs when they cover the whole catalyst surface.

The epitaxial growth on metal catalysts with a face-centered cubic, fcc(111) plane is a promising approach to obtain high quality h-BN films, because the orientation of h-BN grains can be controlled by the underlying fcc(111) lattice. However, the h-BN sheets grown on the fcc(111) planes, such as Cu(111),[25,37] Ir(111),[30] and Ni(111),[22,38] have small grain sizes, typically less than 10 μm. In this paper, we demonstrate the epitaxial CVD growth of large monolayer h-BN grains on Ni(111) deposited on c-plane sapphire with maximum grain sizes up to 500 μm. The use of Ni(111), which has a higher melting point than Cu and Cu-Ni alloys, enabled us to increase the growth temperature, making well-faceted and large triangular h-BN grains on very smooth Ni surface. The growth mechanism of monolayer h-BN is discussed based on the dependences of the temperature, N_2 gas concentration, and pressure during the CVD in combination with structural analysis of the catalyst metal.

Experimental

CVD synthesis of h-BN

A thin Ni(111) film deposited on sapphire and borazine ($B_3N_3H_6$) were used as catalyst substrate and precursor, respectively. A 500 nm-thick Ni film was prepared by radio-frequency (RF) sputtering at ~500 °C using a Ni target (99.99% purity, Kojundo Chemical Laboratory, Japan) on c-plane sapphire (Kyocera, Japan). For comparison, we prepared Cu and Cu-Ni (Ni 20%) alloy films with the same film thickness deposited on c-plane sapphire. For h-BN synthesis, a catalyst substrate was placed in a hot-wall CVD chamber, as illustrated in Figure 1a. We introduced Ar and H_2 gases with a fixed H_2 concentration (4.4 vol%). When we introduced N_2 gas, the amount of Ar was reduced in order to keep the total flow rate and H_2 concentration constant. Prior to the h-BN growth, the substrate was annealed at the growth temperature in the Ar-H_2 flow with the same H_2 concentration (H_2 4.4 vol%) for 1 hour to reduce the Ni surface and to improve the metal crystallinity under controlled pressure (either 1000 Pa or 30 Pa). Then, borazine vapor was introduced to grow h-BN under the same pressure used during the annealing process. The standard growth temperature and pressure were 1100 °C and 1000 Pa, respectively. After a 10-15 min growth period, the Ni(111) substrate was cooled down quickly by taking it out from the heating zone.

As-grown h-BN was transferred to a SiO_2/Si substrate (300 nm SiO_2 thickness) by the polymer-mediated, wet transfer process for further characterizations.[39] The Ni surface was spin-coated with poly(methyl methacrylate) (PMMA), followed by etching in aqueous solution of iron chloride ($FeCl_3$). After thorough washing, the h-BN film was transferred onto a SiO_2/Si substrate, and finally the PMMA was removed by dipping in acetone.

Characterizations

Structures and chemical compositions of the catalyst and h-BN sheet were analyzed by an optical microscope (OM, Nikon Eclipse ME600), a scanning electron microscope (SEM, HITACHI S-4800) equipped with an energy-dispersive X-ray spectroscope (EDS, Bruker QUANTAX FlatQUAD), an atomic force microscope (AFM, Bruker Nanoscope V), and a scanning transmission electron microscope (STEM, JEOL 2100F-based microscope equipped with double delta correctors operating at 60 kV) together with an electron energy-loss spectroscope (EELS, Gatan low-voltage quantum spectrometer). The crystallographic orientation of the Ni substrate was determined by electron backscatter diffraction (EBSD, TSL

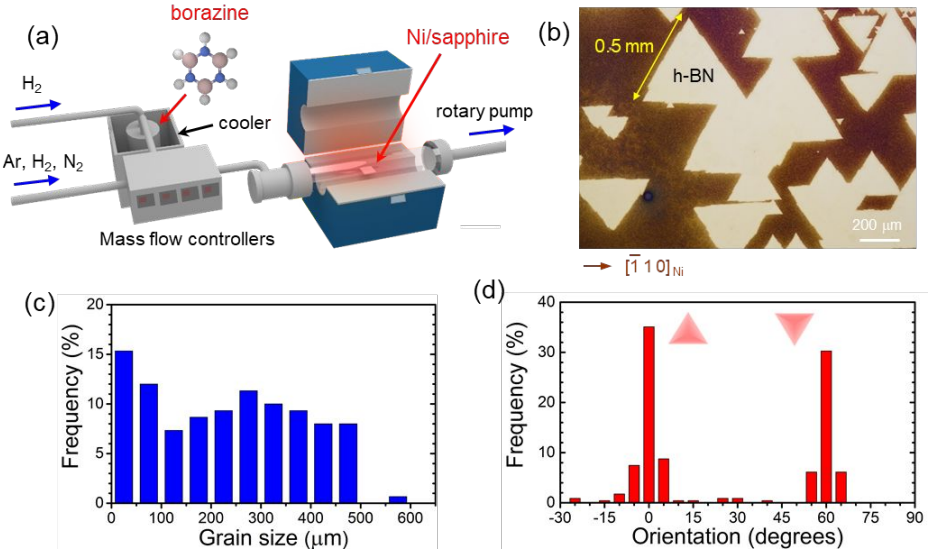

Figure 1. Schematic of the CVD setup used to grow monolayer h-BN. (b) Optical microscope image of h-BN grains grown on Ni(111) film at 1100 °C with 10 vol% N_2 gas. Distributions of size (c) and orientation (d) of h-BN grains made by counting 150 and 228 grains, respectively.

Solutions OIM) attached to a SEM (Zeiss Ultra55). Chemical composition of h-BN was also measured by an X-ray photoelectron spectroscope (XPS, Shimadzu KRATOS Nova). Raman spectra were collected with a Nanofinder 30 (Tokyo Instruments) using 532 nm excitation. The orientation of h-BN grains respect to the Ni(111) substrate was measured by a low-energy electron microscope (LEEM, Elmitec LEEM III) and a photoemission electron microscope (PEEM) in ultrahigh vacuum. A Hg lamp was use as a light source of PEEM.

Results and discussion

Synthesis and characterizations of monolayer h-BN

In this work, we used a liquid precursor, borazine, as h-BN source. The use of borazine allows us to precisely tune the supply rate in the low-pressure CVD system (see Figure 1a). In addition, the h-BN surface can be almost free from nanoparticle impurities. In contrast, ammonia borane, a widely used solid precursor, suffers from the difficulty of controlling the amount of sublimation (*i.e.* the supply rate) and unavoidable side reactions, such as nanoparticle formation due to polymerization.[40]

By utilizing the Ni(111) film deposited on c-plane sapphire as a catalyst, we succeeded in synthesizing large, sub-millimeter h-BN grains, as shown in Figure 1b. Here, we slightly oxidized the as-grown sample at 500 °C for 15 min to visualize the h-BN grains on Ni by the optical microscope. The color of the bare Ni surface became darker due to the surface oxidation, while the Ni below h-BN still exhibited shiny metallic color, because the h-BN can protect Ni from oxidation. The h-BN grains have well-faceted triangular shape with the lateral size exceeding 500 μm. The distribution of the grain size (Figure 1c) verifies the formation of large h-BN grains, with over 70% of the grains being larger than 100 μm. Relatively small grains with lateral sizes below 100 μm were also present (Figure 1b), due to the nucleation proceeding at a late stage of the growth period. Except for these small grains, most of the grains are large with the maximum abundance of the lateral size of ~300 μm (see Figure 1c).

To understand the origin of the large grain growth on the Ni(111) film, we studied the temperature dependence of h-BN grain size. Figure 2a-d shows the optical images of h-BN grown at four different temperatures with a fixed growth time (10 min) and pressure (1000 Pa). Note that the growth time is shorter than that used in Figure 1 (15 min) in order to make well isolated grains for quantitative evaluation of grain density. We found that high CVD temperatures provide three positive impacts on the h-BN grain growth. Firstly, the grain shape becomes sharper with increasing the growth temperature. H-BN grains with sawtooth edges were observed at the lower temperatures (Figure 2a,b), which can be explained by a diffusion-limited growth.[36] Thus, the higher temperatures are supposed to enhance the surface diffusion of h-BN intermediates, making sharp triangular grains.

Second, the grain density drastically decreased with increasing the CVD temperature (see Figure 2a-d). Figure 2e shows an AFM image of the Ni surface that was measured after the annealing in mixed Ar-H_2 flow (H_2 4.4 vol%) at 1100 °C under 1000 Pa for 1 hour. It, thus, corresponds to the Ni surface just before introducing borazine. The Ni surface is very clean with atomic steps running in three directions, reflecting a well-ordered Ni(111) surface. The measured surface roughness (root-mean-square (RMS)) of the Ni(111) film was 0.57 nm, which is smoother than the epitaxial Cu(111) film used for the graphene growth (0.76-1.02 nm).[41] It is highly likely that such smooth and regular Ni surface contributed to the low h-BN nucleation density, as the grain nucleation is known to occur from surface impurity, protruding, and grain boundaries of the metal catalyst surface. In addition, the thermally-activated surface diffusion of h-BN intermediates can also contribute to the observed low grain density.

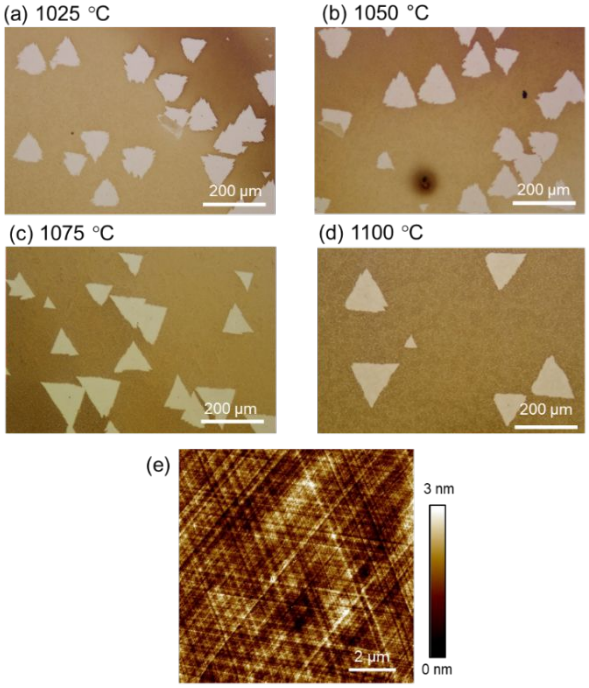

Figure 2. Optical microscope images of h-BN grains grown at 1025 °C (a), 1050 °C (b), 1075 °C (c), and 1100 °C (d). (e) AFM height image of the Ni surface measured after the annealing in Ar-H_2 at 1100 °C.

Thirdly, the h-BN grain size increased with increasing the growth temperature. This can be also accounted for by the enhanced surface diffusion of intermediates on the Ni surface. Therefore, we can conclude that the large h-BN grains shown in Figure 1 was achieved by the combined effects of the high growth temperature (1100 °C) and the smooth and clean surface of the epitaxial Ni(111) film.

It should be noted that the CVD at high temperature (1100 °C) was possible for the Ni film, but not for Cu and Cu-Ni alloy films deposited on c-plane sapphire. This is because the Cu and Cu-Ni alloy films were unstable at this temperature. The result is shown in Supplementary Information, Figure S1. We found that even at 1050 °C severe metal evaporation

occurs for both the Cu and Cu-Ni alloy films, due to the lower melting temperature of Cu (1084 °C) than that of Ni (1455 °C). In particular, the Cu(111) film became non-continuous with many pits reaching to the sapphire surface after the CVD at 1050 °C. Figure S1c shows the SEM images at different positions of the Cu-Ni alloy film after the CVD process. The Cu evaporation also occurred in this alloy film, resulting in the inhomogeneous distribution of Cu atoms in the film. Consequently, small h-BN grains with a lateral size <10 μm were observed at certain positions of the substrate (Figure S1b). The Cu evaporation was found to occur more predominantly at the upstream of the substrate (Figure S1c). This infers that the Cu evaporation is enhanced by borazine vapor. In stark contrast, pure Ni(111) films were found to be stable at the higher CVD temperature of 1100 °C, as shown in Figure S1d.

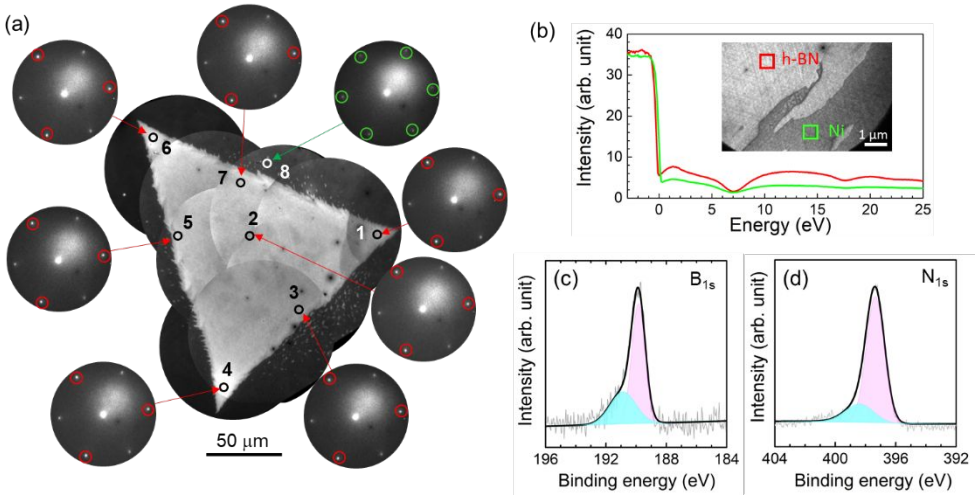

Figure 3. (a) PEEM image of an as-grown h-BN grain on Ni and electron diffraction patterns measured at the marked positions. (b) Electron reflectivity curves taken at the h-BN and bare Ni areas. Inset shows a PEEM image where the reflectivity curves were collected. (c,d) High resolution XPS spectra of B and N elements. Grey lines show the original spectra, and bold lines show the fitted curves using pink and light blue peaks.

As seen in Figure 1b, the h-BN grains are aligned on the Ni(111) surface, with their grain edges parallel to the $[\bar{1}10]$ axis of the Ni film. The angle distribution is plotted in Figure 1d. This graph shows that there are two preferred orientations in the h-BN grains grown on the Ni(111) surface. These results strongly suggest the epitaxial growth of monolayer h-BN grains on the Ni(111) which is also epitaxially deposited on sapphire. These two preferred orientations correspond to different registries of h-BN on Ni(111) surface where one B atom occupies the hexagonal close packed (hcp) site and the other on top of fcc site.[42,43] The atomic models are displayed in Figure S2. As the energy difference between these two registries is very small, the h-BN grains have the two observed main orientations on the Ni(111) surface (see Figure 1d). We note that the sapphire substrate enables the large-area deposition of a Ni(111) thin film, allowing to grow large area, highly aligned h-BN, which is crucial for many applications. In addition, the grain size of CVD-grown h-BN obtained in this work is the largest among the values reported so far, as compared in Figure S3.

Figure 3a shows a PEEM image and electron diffraction patterns taken at the marked positions including that of the bare Ni surface (position 8). Here, the merged PEEM image is displayed, because the grain size is large. A partially merged bright-field LEEM image can be also found in Supplementary Figure S4. Within the h-BN grain (at the positions 1-7 of Figure 3a), a set of six diffraction spots was observed of which three spots (highlighted in red) are much brighter than others. These bright triangular spots seen at the positions 1-7 confirm the growth of h-BN having 3-fold symmetry. Moreover, the orientation of the triangular spots is the same within the whole grain, proving the single crystalline nature of the h-BN.

The bare Ni surface (position 8) showed six diffraction spots with the same intensity, expected for the Ni(111) surface. As the lattice constants of h-BN (0.256 nm) and Ni(111) (0.249 nm) are very close (lattice mismatch is ~3%), the six diffraction spots seen at the positions 1-7 originate in both h-BN and Ni(111) lattices.[31] We note that the diffraction spots at the position 8 (from bare Ni) are much weaker than those from h-BN/Ni. Such weak diffraction signal from the position 8 is caused by oxidation of the Ni surface, because the bare Ni is not protected from air during the transfer to LEEM chamber. This agrees with the observations from the oxidized as-grown samples (for example, Figure 1b), showing that h-BN acts as a good gas barrier film preventing the oxidation of the Ni(111) surface.

It is worthwhile to note that the orientation of the three intense diffraction spots seen at the positions 1-7 (highlighted in red in Figure 3a), is consistent with that of the six spots taken at the position 8 (highlighted in green). This proves the epitaxial growth of h-BN, whose orientation is registered by the underlying Ni(111) surface. The observed alignment can be explained by the strong interaction between Ni 3d orbitals and h-BN π orbitals.[44]

Electron reflectivity curves were also measured for the as-grown sample, as they can be used to identify 2D materials and to determine the number of layers. Figure 3b shows the reflectivity curves collected at the areas shown in the inset. While the bare Ni surface gave a featureless flat curve, the h-BN grain showed a characteristic curve with two dips at around 7 and 18 eV, being consistent with the monolayer nature of the h-BN.[29] A similar result was obtained for a different h-BN grain grown on the Ni(111) (Figure S5).

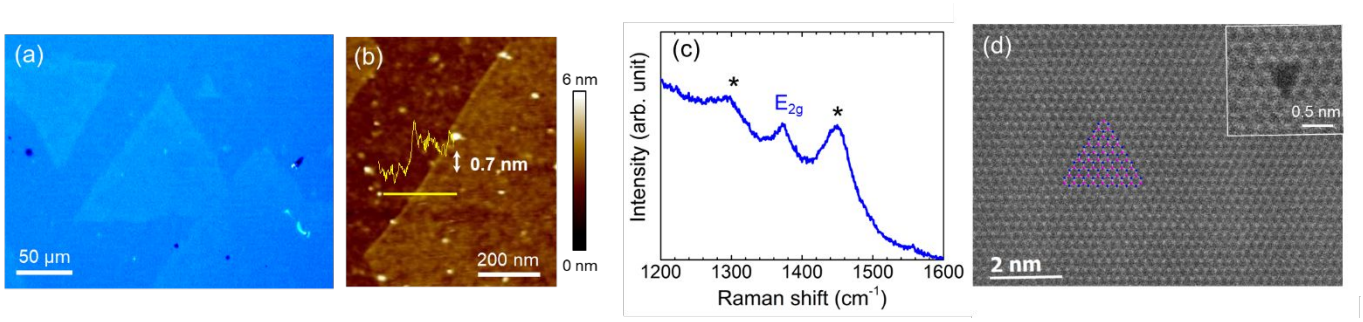

Figure 4. (a) Optical and (b) AFM images of transferred h-BN on SiO_2/Si substrate. (c) Raman spectrum of the transferred h-BN. Asterisks indicate the peaks originate from the substrate.[35] (d) STEM image of monolayer h-BN with the atomic model (pink and blue correspond to B and N atoms, respectively). Inset shows a hole created by an electron beam used in the STEM measurement.

Figures 3c and 3d show the XPS spectra of B_{1s} and N_{1s} elements, respectively, collected from the as-grown sample. We performed peak fitting and found that both peaks are consisting of two peaks, highlighted in pink and blue, in Figure 3c,d. The lower energy peaks (189.9 and 397.4 eV) are assigned to sp^2-hybridized boron nitride, corresponding to monolayer h-BN. On the other hand, the higher energy peaks (190.9 and 398.4 eV) are assigned to sp^3 species.[25,45] The B:N ratio of our h-BN film determined from the intensities of the sp^2 peaks was 1:0.98, very close to the stoichiometric ratio of h-BN.

As grown h-BN films were transferred onto SiO_2/Si substrates for further characterizations. Figure 4a shows an optical image of the transferred h-BN. Although h-BN is known to show much weaker optical contrast compared to graphene,[46] we could recognize the presence of transferred h-BN grains by enhancing the image contrast. The AFM image, shown in Figure 4b, indicates a 0.7 nm thickness, corresponding to monolayer height, which is consistent with the low optical contrast and electron reflectivity curve (see Figures 3b and 4a). The Raman spectrum of the transferred film (Figure 4c) exhibited a characteristic E_{2g} band at ~1372 cm^{-1}, assigned to the in-plane lattice vibration of h-BN. It has been reported that the E_{2g} band shifts from ~1366 cm^{-1} to ~1370 cm^{-1} when thinning down from bulk to monolayer.[46] Also, the E_{2g} band becomes weaker and broader with decreasing h-BN thickness.[46] Therefore, the observed Raman signal also supports the formation of monolayer h-BN on Ni(111) catalyst.

Atomic scale STEM measurement was performed by transferring h-BN from Ni onto a TEM grid. As shown in Figure 4d, we observed a hexagonal lattice that can be assigned to monolayer h-BN. The EELS analysis confirmed the presence of both B and N in the specimen (Figure S6). As the contrast in STEM is proportional to the atomic number, the locations of N atoms (blue) and B atoms (pink) can be assigned straightforwardly in monolayer h-BN lattice. Interestingly, a typical triangular vacancy V_{N+3B} (missing of one nitrogen and three boron atoms) was created by an electron beam and left N terminating edges, as shown in Figure 4d inset.[47] The N termination is more energetically stable than B termination in monolayer h-BN, which is also predicted by density functional theory (DFT) calculation.[48]

Growth mechanism

Figure 5 displays the evolution of crystal structure of the Ni film investigated by EBSD. We measured the EBSD at each step of h-BN growth; after the magnetron sputtering, after annealing in Ar-H_2 at 1100 °C (1000 Pa), and after h-BN growth with borazine vapor at the same temperature and pressure. All the out-of-plane images (Figure 5a,c,e) showed blue color corresponding to a fcc(111) plane normal to the Ni surface. However, there are clear differences in each blue contrast. The as-sputtered Ni film has polycrystalline structure with very small Ni grain size, less than 10 μm (Figure 5a). The in-plane pole figure showed two sets of three spots with slightly different intensities (Figure 5b). These results indicate that the Ni(111) film is consisting of a number of small twin crystal grains (<10 μm). The formation of the twin structure in fcc(111) metals, such as Cu(111) and Ni(111), on c-plane sapphire has been widely recognized,[49,50] because the 3-fold symmetry of fcc(111) metal does not completely match with the 6-fold sapphire (0001) surface.

After the annealing in the mixed Ar-H_2 flow at the CVD temperature (1100 °C) for 1 hour, the Ni grains became larger (Figure 5c), as compared with the as-sputtered film. However, the twin structure still remained, as can be seen by two different blue contrasts in Figure 5c. This is also recognized by the remaining a set of three spots highlighted by the grey arrows in Figure 5d. Thus, the high-temperature H_2 annealing

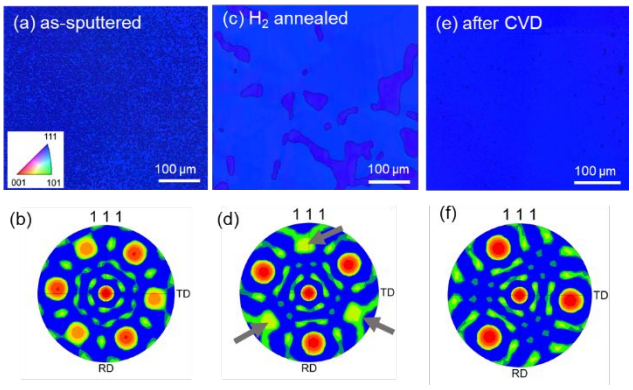

Figure 5. Crystallographic characterization of a Ni film deposited on c-plane sapphire. (a,b) After sputtering deposition of a Ni film. (c,d) After annealing in Ar-H_2 gas flow, (e,f) After h-BN growth with borazine. (a,c,e) Crystalline plane orientation of the Ni film normal to the surface. (b,d,f) [111] pole figures.

increases the Ni crystallinity, but it is difficult to convert the Ni film to single crystal.

Interestingly, the Ni film after the h-BN growth showed a very uniform blue contrast in the out-plane image (Figure 5e), indicating that the twin structure completely disappeared during the h-BN growth period. This twin-free structure was also confirmed by the pole figure (Figure 5f), in which only one set of three spots remains. This strongly suggests that the Ni(111) film experiences the structural reconstruction during the supply of borazine at the high temperature.

Being different from the Cu(111)/sapphire system that shows the twin structure even after the graphene growth,[48] the Ni/sapphire showed a drastic change in the film morphology after the h-BN growth. This result signifies that borazine plays a crucial role in the reconstruction of the Ni(111) film. This phenomenon could be related to the dissolution of B atoms in the Ni film, because the solubility of B is relatively high (~0.3%) compared to that of N (~0.004%) at high temperature.[51] We speculate that the dissolution-segregation process of B atoms induces the structural change of the Ni film, increasing the Ni grain size and aligning the in-plane lattice orientation. This structural change during the h-BN growth was also observed for a Fe-Ni alloy film.[52] Assuming the higher dissolution of B atoms, it is speculated that the supply of N atoms is more important for the effective synthesis of large h-BN grains, because the Ni film can act as a B reservoir. The higher sp^3 component of B atom than that of N atom observed in the XPS spectra (light blue peaks in Figure 3c,d) can be related to the dissolved B atoms in the Ni film. The low N solubility, on the other hand, leads to the preferential growth of monolayer h-BN due to the self-limiting mechanism, as was observed for the monolayer growth of graphene and h-BN on Cu.[25,32]

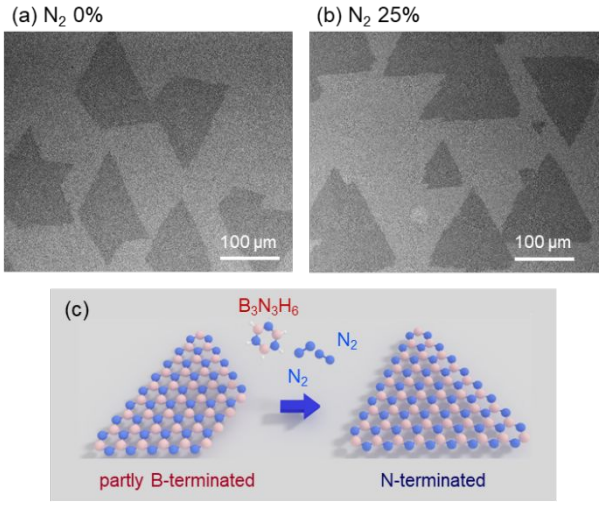

Figure 6. SEM images of h-BN grown (a) without N_2 gas and (b) with 25 vol% N_2 gas added during the borazine supply. (c) Schematic of the influence of N_2 gas on the h-BN grain shape. Pink and blue atoms correspond to B and N atoms, respectively.

Therefore, in the next step, we investigated the influence of N_2 gas added to borazine vapor during the h-BN growth. Figures 6 and S7 show the influence of N_2 gas on the h-BN grain shape. In the absence of N_2 gas (*i.e.* Ar and H_2 gas flow), the h-BN grains possess irregular triangle shapes with partly truncated edges (Figure 6a,c). The previous literatures reported the truncated grain edges stem from the partial termination with B atoms in addition to the stable N-termination.[21,24]. Thus, the observed truncated edges can be associated with the B-rich Ni film. When we introduced N_2 gas with concentrations over 10 vol%, the h-BN grain changed to have a perfect triangular shape (see Figures 6b and S7), which is explained by the edge termination with N atoms. As dissociation of a N_2 molecule is not likely to occur due to its high stability, we speculate that N_2 gas suppresses the desorption of adsorbed N atoms from the Ni(111) surface. This would increase the concentration of N atoms on the Ni surface, resulting in the formation of triangular h-BN grains with sharp edges (Figure 6c).

Influence of the pressure during the CVD on h-BN growth was also studied. We reduced the pressure from 1000 Pa to 30 Pa. As shown in Figure S8, the Ni surface became irregular and distorted compared with that 1000 Pa sample. This is accounted for by the evaporation of Ni due to low pressure condition at high temperature (1100 °C). The rougher surface obtained at 30 Pa leads to an increase of the h-BN nucleation density. Figure S8c shows the SEM image after the CVD growth at 30 Pa. The Ni surface was fully covered with h-BN, signifying the high nucleation density.

There are many steps in the h-BN growth process; catalytic dissociation of borazine, diffusion of precursors on the Ni surface, dissolution of B atoms in the Ni bulk, nucleation as h-BN, and development of a h-BN grain. Compared with graphene,[41] it is more difficult to discuss quantitatively, because two elements, B and N, are involved in the growth and their solubilities in Ni bulk are different. Figure 7 shows the semi-log plots of temperature dependences of the grain density and size, from which we calculated the activation energies by linear fitting. The relatively high activation energy determined for the h-BN nucleation (2.2 eV) indicates that the h-BN growth is a thermally activated process. Being different from the graphene growth, activation energy for the grain growth of h-BN is much smaller (0.6 eV). This may reflect the ionic nature of h-BN, because free N- or B-terminated edges attract another element due to the polarized B-N bonds. Therefore, low energy may be sufficient to attach new B/N atoms to free N/B edges, once a h-BN nucleus is formed on the Ni(111) surface.

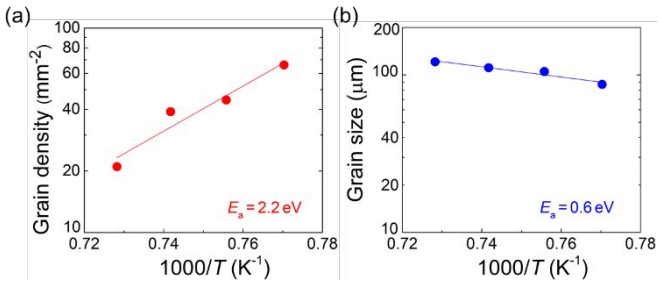

Figure 7. Temperature dependences of density and lateral size of h-BN grains. The activation energy is also indicated in each graph.

Conclusions

Large and epitaxially aligned monolayer h-BN grains were successfully synthesised on a Ni(111) thin film which was also epitaxially deposited on c-plane sapphire. We found that the reaction temperature, N_2 gas concentration, and pressure strongly affect the h-BN growth. In particular, the high growth temperature (1100 °C) was found to be essential to obtain large grains up to 500 μm with a well-faceted structure. The thermally stable Ni(111) gave smooth and clean surface and at the same time enhanced the surface diffusion of the intermediate species, assisting the large grain growth. Other catalysts, Cu and Cu-Ni alloy films, were not stable at such high temperature due to significant evaporation of Cu atoms. The present study is expected to contribute to the understanding of the growth mechanism and to the effective synthesis of high-quality monolayer h-BN.

Conflicts of interest

There are no conflicts to declare.

Acknowledgements

This work was supported by JSPS KAKENHI grant numbers JP17K19036 and JP18H03864 and JST CREST grant number JPMJCR18I1. A part of this work was conducted at the AIST Nano-Processing Facility, supported by "Nanotechnology Platform Program" of the Ministry of Education, Culture, Sports, Science and Technology (MEXT), Japan.

Notes and references

1 K. S. Novoselov, A. K. Geim, S. V. Morozov, D. Jiang, Y. Zhang, S. V. Dubonos, I. V. Grigorieva, and A. A. Firsov, *Science*, 2004, **306**, 666.
2 K. Zhang, Y. Feng, F. Wang, Z. Yang, and J. Wang, *J. Mater. Chem. C*, 2017, **5**, 11992.
3 M. Topsakal, E. Aktürk, and S. Ciraci, *Phys. Rev. B*, 2009, **79**, 115442.
4 L. H. Li, J. Cervenka, K. Watanabe, T. Taniguchi, and Y. Chen, *ACS Nano*, 2014, **8**, 1457.
5 A. Falin, Q. Cai, E. J. G. Santos, D. Scullion, D. Qian, R. Zhang, Z. Yang, S. Huang, K. Watanabe, T. Taniguchi, M. R. Barnett, Y. Chen, R. S. Ruoff, and L. H. Li, *Nat. Commun.*, 2017, **8**, 15815.
6 Y. Kubota, K. Watanabe, O. Tsuda, and T. Taniguchi, *Science*, 2007, **317**, 932.
7 M. Piquemal-Banci, R. Galceran, S. Caneva, M.-B. Martin, R. S. Weatherup, P. R. Kidambi, K. Bouzehouane, S. Xavier, A. Anane, F. Petroff, A. Fert, J. Robertson, S. Hofmann, B. Dlubak, and P. Seneor, *Appl. Phys. Lett.*, 2016, **108**, 102404.
8 W. Luo, L. Zhou, K. Fu, Z. Yang, J. Wan, M. Manno, Y. Yao, H. Zhu, B. Yang, and L. Hu, *Nano Lett.*, 2015, **15**, 6149.
9 S. Hu, M. Lozada-Hidalgo, F. C. Wang, A. Mishchenko, F. Schedin, R. R. Nair, E. W. Hill, D. W. Boukhvalov, M. I. Katsnelson, R. a. W. Dryfe, I. V. Grigorieva, H. A. Wu, and A. K. Geim, *Nature*, 2014, **516**, 227.
10 X. Ling, W. Fang, Y.-H. Lee, P. T. Araujo, X. Zhang, J. F. Rodriguez-Nieva, Y. Lin, J. Zhang, J. Kong, and M. S. Dresselhaus, *Nano Lett.*, 2014, **14**, 3033.
11 G.-H. Lee, Y.-J. Yu, X. Cui, N. Petrone, C.-H. Lee, M. S. Choi, D.-Y. Lee, C. Lee, W. J. Yoo, K. Watanabe, T. Taniguchi, C. Nuckolls, P. Kim and J. Hone, *ACS Nano*, 2013, **7**, 7931.
12 C. R. Dean, A. F. Young, I. Meric, C. Lee, L. Wang, S. Sorgenfrei, K. Watanabe, T. Taniguchi, P. Kim, K. L. Shepard, and J. Hone, *Nat. Nanotechnol.*, 2010, **5**, 722.
13 G. Giovannetti, P. A. Khomyakov, G. Brocks, P. J. Kelly, and J. van den Brink, *Phys. Rev. B*, 2007, **76**, 073103.
14 R. A. Doganov, E. C. T. O'Farrell, S. P. Koenig, Y. Yeo, A. Ziletti, A. Carvalho, D. K. Campbell, D. F. Coker, K. Watanabe, T. Taniguchi, A. H. C. Neto, and B. Özyilmaz, *Nat. Commun.*, 2015, **6**, 6647.
15 L. Shen, Y. Zhao, Y. Wang, R. Song, Q. Yao, S. Chen, and Y. Chai, *J. Mater. Chem. A*, 2016, **4**, 5044.
16 M. H. Khan, H. K. Liu, X. Sun, Y. Yamauchi, Y. Bando, D. Golberg, and Z. Huang, *Mater. Today*, 2017, **20**, 611.
17 A-R. Jang, S. Hong, C. Hyun, S. I. Yoon, G. Kim, H. Y. Jeong, T. J. Shin, S. O. Park, K. Wong, S. K. Kwak, N. Park, K. Yu, E. Choi, A. Mishchenko, F. Withers, K. S. Novoselov, H. Lim, and H. S. Shin, *Nano Lett.*, 2016, .**16**, 3360.
18 S. Behura, P. Nguyen, R. Debbarma, S. Che, M. R. Seacrist, and V. Berry, *ACS Nano*, 2017, **11**, 4985.
19 Q. Wu, J.-H. Park, S. Park, S. J. Jung, H. Suh, N. Park, W. Wongwiriyapan, S. Lee, Y. H. Lee, and Y. J. Song, *Sci. Rep.*, 2015, **5**, 16159.
20 S. Sinha, Y. Takabayashi, H. Shinohara, and R. Kitaura, *2D Mater.*, 2016, **3**, 035010.
21 Y. Stehle, H. M. Meyer, R. R. Unocic, M. Kidder, G. Polizos, P. G. Datskos, R. Jackson, S. N. Smirnov, and I. V. Vlassiouk, *Chem. Mater.*, 2015, **27**, 8041.
22 G. E. Wood, A. J. Marsden, J. J. Mudd, M. Walker, M. Asensio, J. Avila, K. Chen, G. R. Bell, and N. R. Wilson, *2D Mater.*, 2015, **2**, 025003.
23 K. K. Kim, A. Hsu, X. Jia, S. M. Kim, Y. Shi, M. Hofmann, D. Nezich, J. F. Rodriguez-Nieva, M. Dresselhaus, T. Palacios, and J. Kong, *Nano Lett.*, 2012, **12**, 161.
24 R. Y. Tay, M. H. Griep, G. Mallick, S. H. Tsang, R. S. Singh, T. Tumlin, E. H. T. Teo, and S. P. Karna, Nano Lett., 2014, 14, 839.
25 Y. Uchida, T. Iwaizako, S. Mizuno, M. Tsuji, and H. Ago, *Phys. Chem. Chem. Phys.*, 2017, **19**, 8230.
26 G. Kim, A.-R. Jang, H. Y. Jeong, Z. Lee, D. J. Kang, and H. S. Shin, *Nano Lett.*, 2013, **13**, 1834.
27 J.-H. Park, J. C. Park, S. J. Yun, H. Kim, D. H. Luong, S. M. Kim, S. H. Choi, W. Yang, J. Kong, K. K. Kim, and Y. H. Lee, *ACS Nano*, 2014, **8**, 8520.
28 Z. Zhang, X. Ji, J. Shi, X. Zhou, S. Zhang, Y. Hou, Y. Qi, Q. Fang, Q. Ji, Y. Zhang, M. Hong, P. Yang, X. Liu, Q. Zhang, L. Liao, C. Jin, Z. Liu, and Y. Zhang, *ACS Nano*, 2017, **11**, 4328.
29 C. M. Orofeo, S. Suzuki, H. Kageshima, and H. Hibino, *Nano Res.*, 2013, **6**, 335.
30 F. H. Farwick zum Hagen, D. M. Zimmermann, C. C. Silva, C. Schlueter, N. Atodiresei, W. Jolie, A. J. Martínez-Galera, D. Dombrowski, U. A. Schröder, M. Will, P. Lazić, V. Caciuc, S. Blügel, T.-L. Lee, T. Michely, and C. Busse, *ACS Nano*, 2016, **10**, 11012.
31 Y. Yang, Q. Fu, H. Li, M. Wei, J. Xiao, W. Wei, and X. Bao, *ACS Nano*, 2015, **9**, 11589.
32 X. Li, W. Cai, J. An, S. Kim, J. Nah, D. Yang, R. Piner, A. Velamakanni, I. Jung, E. Tutuc, S. K. Banerjee, L. Colombo, and R. S. Ruoff, *Science*, 2009, **324**, 1312.
33 B. Mortazavi and G. Cuniberti, *RSC Adv.*, 2014, 4, 19137.
34 R.-J. Chang, X. Wang, S. Wang, Y. Sheng, B. Porter, H. Bhaskaran, and J. H. Warner, *Chem. Mater.*, 2017, **29**, 6252.
35 G. Lu, T. Wu, Q. Yuan, H. Wang, H. Wang, F. Ding, X. Xie, and M. Jiang, *Nat. Commun.*, 2015, **6**, 6160.
36 S. Caneva, R. S. Weatherup, B. C. Bayer, B. Brennan, S. J. Spencer, K. Mingard, A. Cabrero-Vilatela, C. Baehtz, A. J. Pollard, and S. Hofmann, *Nano Lett.*, 2015, **15**, 1867.

37 S. Joshi, D. Ecija, R. Koitz, M. Iannuzzi, A. P. Seitsonen, J. Hutter, H. Sachdev, S. Vijayaraghavan, F. Bischoff, K. Seufert, J. V. Barth, and W. Auwärter, *Nano Lett.*, 2012, **12**, 5821.
38 W. Auwärter, H. U. Suter, H. Sachdev, and T. Greber, *Chem. Mater.*, 2004, **16**, 343.
39 H. Ago, K. Kawahara, Y. Ogawa, S. Tanoue, M. A. Bissett, M. Tsuji, H. Sakaguchi, R. J. Koch, F. Fromm, T. Seyller, K. Komatsu, and K. Tsukagoshi, *Appl. Phys. Express*, 2013, **6**, 075101.
40 J. Han, J.-Y. Lee, H. Kwon, and J.-S. Yeo, *Nanotechnology*, 2014, **25**, 145604.
41 H. Ago, Y. Ohta, H. Hibino, D. Yoshimura, R. Takizawa, Y. Uchida, M. Tsuji, T. Okajima, H. Mitani and S. Mizuno, *Chem. Mater.*, 2015, **27**, 5377.
42 W. Auwärter, M. Muntwiler, J. Osterwalder and T. Greber, *Surf. Sci.*, 2003, **545**, L735–L74
43 J. Gómez Díaz, Y. Ding, R. Koitz, A. P. Seitsonen, M. Iannuzzi and J. Hutter, *Theor. Chem. Acc.*, 2013, **132**, 1350.
44 A. B. Preobrajenski, A. S. Vinogradov, and N. Mårtensson, *Surf. Sci.*, 2005, **582**, 21.
45 H. Tian, A. Khanaki, P. Das, R. Zheng, Z. Cui, Y. He, W. Shi, Z. Xu, R. Lake, and J. Liu, *Nano Lett.*, 2018, **18**, 3352.
46 R. V. Gorbachev, I. Riaz, R. R. Nair, R. Jalil, L. Britnell, B. D. Belle, E. W. Hill, K. S. Novoselov, K. Watanabe, T. Taniguchi, A. K. Geim, and P. Blake, *Small*, 2011, **7**, 465.
47 C. Jin, F. Lin, K. Suenaga, and S. Iijima, *Phys. Rev. Lett.*, 2009, **102**, 195505.
48 Y. Liu, S. Bhowmick and B. I. Yakobson, *Nano Lett.*, 2011, **11**, 3113.
49 B. Hu, H. Ago, Y. Ito, K. Kawahara, M. Tsuji, E. Magome, K. Sumitani, N. Mizuta, K. Ikeda, and S. Mizuno, *Carbon*, 2012, **50**, 57.
50 Z. Fogarassy, G. Dobrik, L. K. Varga, L. P. Biró, and J. L. Lábár, *Thin Solid Films*, 2010, **539**, 96.
51 S. Suzuki, R. M. Pallares, and H. Hibino, *J. Phys. Appl. Phys.*, 2012, **45**, 385304.
52 Y. Uchida, S. Nakandakari, K. Kawahara, S. Yamasaki, M. Mitsuhara, and H. Ago, *ACS Nano*, 2018, **12**, 6236.

TOC graphics